Nanotubes Made from Deeply Undercooled Cryolite/Alumina Melts

by **Michal Korenko***[a]), **Marián Kucharík**[a]), **Jozef Vincenc Oboňa**[b])[c]), **Dušan Janičkovič**[d]), **Rosa Córdoba**[c]), **José María De Teresa**[e]), and **Blanka Kubíková**[a])

[a]) Institute of Inorganic Chemistry, Slovak Academy of Sciences, Dubravska cesta 9, SK-84536 Bratislava (phone: +421259410463; fax: +421259410444; e-mail: Michal.Korenko@savba.sk)

[b]) Institute of Electrical Engineering, Slovak Academy of Sciences, Dubravska cesta 9, SK-84536 Bratislava

[c]) Instituto Universitario de Nanociencia de Aragón, University of Zaragoza, Pedro Cerbuna 12, ES-50009 Zaragoza

[d]) Institute of Physics, Slovak Academy of Sciences, Dubravska cesta 9, SK-84536 Bratislava

[e]) Instituto de Ciencia de Materiales de Aragón, CSIC-University of Zaragoza, ES-50009 Zaragoza

The rapid-solidification processing (by a cooling rate of $10^5 - 10^6$ K/s) was used for the preparation of deeply undercooled cryolite/alumina (Na_3AlF_6/Al_2O_3) melts. We found a mass of nanotubes on the surface of these undercooled melts. The nanotubes were preferentially located on the defect places of the surface with the following approximate dimensions: base $\approx 100 \times 100$ nm, length ≈ 1000 nm. The solidified samples with the nanotubes on the surface were analyzed by scanning electron microscopy (SEM), energy-dispersive X-ray spectroscopy (EDX), X-ray diffraction (XRD), and infrared spectroscopy (IR).

Introduction. – Since the discovery of carbon nanotubes [1], tubular nanocrystals have attracted extensive attention over the past decade for their potential technological applications. Especially, tubular inorganic structures with a quadrate cross section are considered to exhibit outstanding properties, which are interesting not only for fundamental research but also for the construction of one-dimensional structures in optoelectronics (*e.g.*, optical-resonance cavities) as well as nanodevices, microreactors, sensors, fluid flow, and distribution channels in microfluidics [2][3]. However, reports on such types of tubular structures are rare.

In the present article, we describe nanotubes with a quadrate cross section, which we accidentally found on the surface of deeply undercooled cryolite (Na_3AlF_6)/alumina (Al_2O_3) melts, prepared by the rapid solidification processing (RSP) technique.

Cryolite and alumina are the main constituents of the electrolyte for the industrial production of primary aluminium (by the so-called *Hall–Héroult* process). Although, the cryolite/alumina melts are the subjects of long-standing immense scientific research, there is no evidence in the literature for the connection of the term 'cryolite/alumina systems' with 'nanotubes' (or nano structures).

The RSP technology is most often used in a different field of material engineering than for cryolite/alumina melts, *i.e.*, for the preparation of special amorphous materials (especially glassy metals) with interesting physical and chemical properties (mechanical and magnetic properties, semiconductivity, ferroelectricity, superconductivity and

optical properties, corrosion resistance, catalytic activity, *etc.*). The RSP technique is based on the 'gun' technique in which a small droplet of molten material impacts at high velocity on a chill surface, resulting in a nonuniform 'splat' of solidified material (for detailed information, see [4]). The cooling rate associated with such a process is estimated to be in the range from 10^5 to 10^6 K/s, certainly very rapid in comparison with conventional solidification rates, which are 10^2 K/s or less.

The RSP was rarely used for the preparation of nonmetal materials (mainly different types of oxides). There are only two papers related to fluorides [5][6]. In the first case, they were Zr–Ba–Y–Al fluoride glasses; in the second case, it was PbF_2–AlF glass. In both compounds, the fluoride glasses (prepared by RSP) have shown good IR transmittance properties.

Despite the fact that the preparation of many inorganic compounds with tubular morphology was demonstrated [7] (soon after the identification of carbon nanotubes [1]), reports on quadrate tubular structures are rare (SnO_2 [2][8][9], PbS [10], MoO_2 [11]). We found no reports in the literature about the nanomorphology related to fluoride systems.

Results and Discussion. – The products of the rapid quenching of cryolite/alumina melts can be divided into two different groups. The first group consisted of glassy, in the whole bulk transparent, and fragile needles (length *ca.* 5 mm, diameter *ca.* 1 mm). The second one consisted of stony, white aggregates of different shapes. The nanotubes were only observed in the second group, on the surface of aggregates. In the following, we will merely present the analysis of these aggregates, and despite of this, we will use the term undercooled melts.

Scanning-Electron-Miscroscopy (SEM) *Analysis.* The SEM pictures of the surface of a deeply undercooled cryolite/alumina melt (10 wt.-% Al_2O_3) are shown in *Figs. 1* and *2*. The forests of nanotubes can be seen. The nanotubes are located just on the defect places of the surface (tectonic disruptions, cracks, and gaps, *Fig. 2*, *B9* and *B10*). The tubes have usually a square shape in cross-section, which is clearly seen in *Fig. 1*, *B1* and *B2*, and in *Fig. 2* (base *ca.* 100×100 nm, length *ca.* 1000 nm). However, there is also a fluctuation of the tubes geometry. Thus, among nanotubes with a larger base of prism (*Fig. 1*, *B3* and *B4*), a different cavity shape of the nanotubes as well as defects on the side walls are observed. The larger area of prisms could be explained by a different diameter of 'crystallization seeds', cavity shape by vaporization of any component of the melt (we consider $NaAlF_4$) inside the tube, and defects within the side walls by failures in the initial phase of growing.

Although the tubes are in fact hollow prisms, we are rather using the term tubes. The nanotubes were found on the surface of all alumina-containing deeply undercooled melts. We did not observe the nanotubes, or any similar structure, on the surface of pure cryolite samples.

The feature of the nanotubes showed in *Figs. 1* and *2* is partly similar to the hollow rectangular nanotubes made from SnO_2 [2][8][9]. However, the reported SnO_2 tubular structures are much bigger (base of cross-serction *ca.* 500–1000 nm).

Energy-Dispersive X-Ray Spectroscopy (EDX) *Analysis.* The results of the EDX analysis (*Zeiss*, model *EVO 40 HV*, *Carl Zeiss SMT AG*, Germany) established that the samples (10, 20, and 30 wt.-% Al_2O_3) contain a relatively high amount of C, besides the

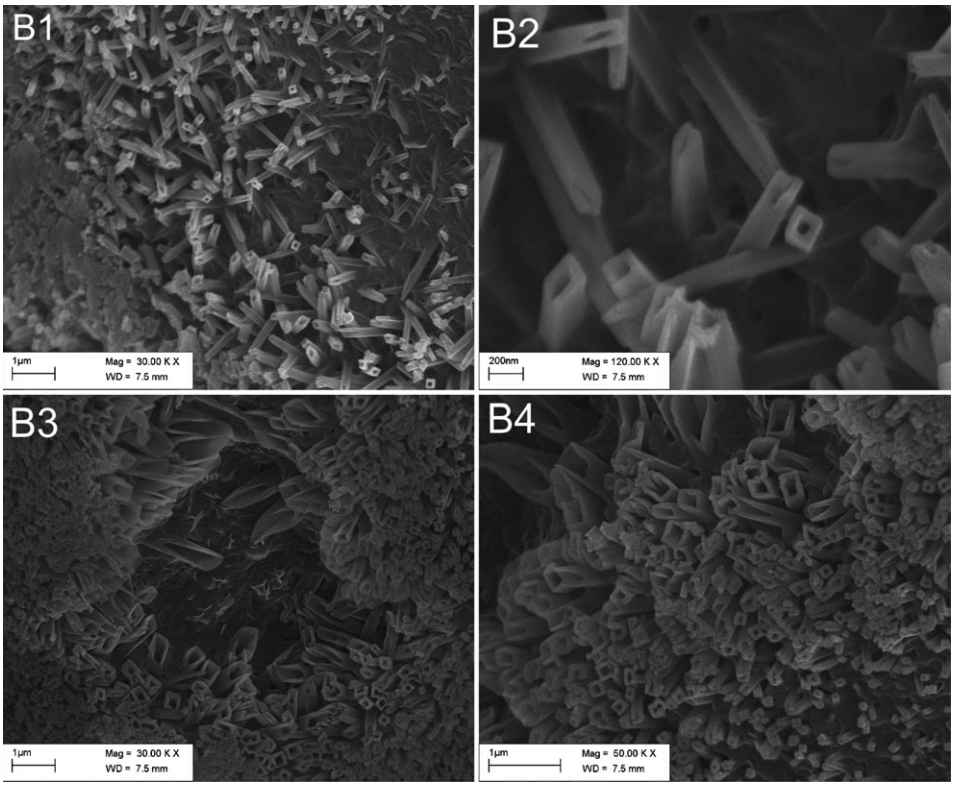

Fig. 1. *SEM Images of the surface of the deeply undercooled cryolite/alumina melt* (10 wt.-% of Al_2O_3) (*Zeiss* model *EVO 40 HV*, *Carl Zeiss SMT AG*, Germany). Magnification: *B1* 30000 ×, *B2* 120000 ×, *B3* 30000 ×, and *B4* 50000 ×.

elements coming from cryolite and alumina (Na, Al, F, and O). The subsequent open-air annealing at 600° (5 h) of the nanotubes (sample with 10 wt.-% of Al_2O_3) eliminated the C from the sample without any impact on the surface nanomorphology (*Fig. 3*). It suggests that the C in the sample is only an impurity coming into the system from the graphite crucible during the quenching process. However, we can not completely exclude its role as a crystal seed during the formation of the nanotubes.

Due to the partial crystallization of the quenched melt in the form of nanotubes (mainly inside cracks), EDX analysis was considered appropriate to investigate the content differences in the bulk material and the nanotubes. We used two different methods for the evaluation by EDX. The first method involves an *EVO-40-HV* (*Carl Zeiss SMT AG*, Germany) equipment in the configuration displayed by *Fig. 4*. The thickness of the nanotubes 'layer' ranges from 500 nm to 1 µm. During the EDX measurement, an electron beam (e-beam) perpendicular to the sample surface and a 25 kV accelerating voltage were applied.

The second method involves a 30 kV accelerating voltage as well as an e-beam tilted by 52° and pointing the surface of the side wall of a 500 nm wide lamella directly on the

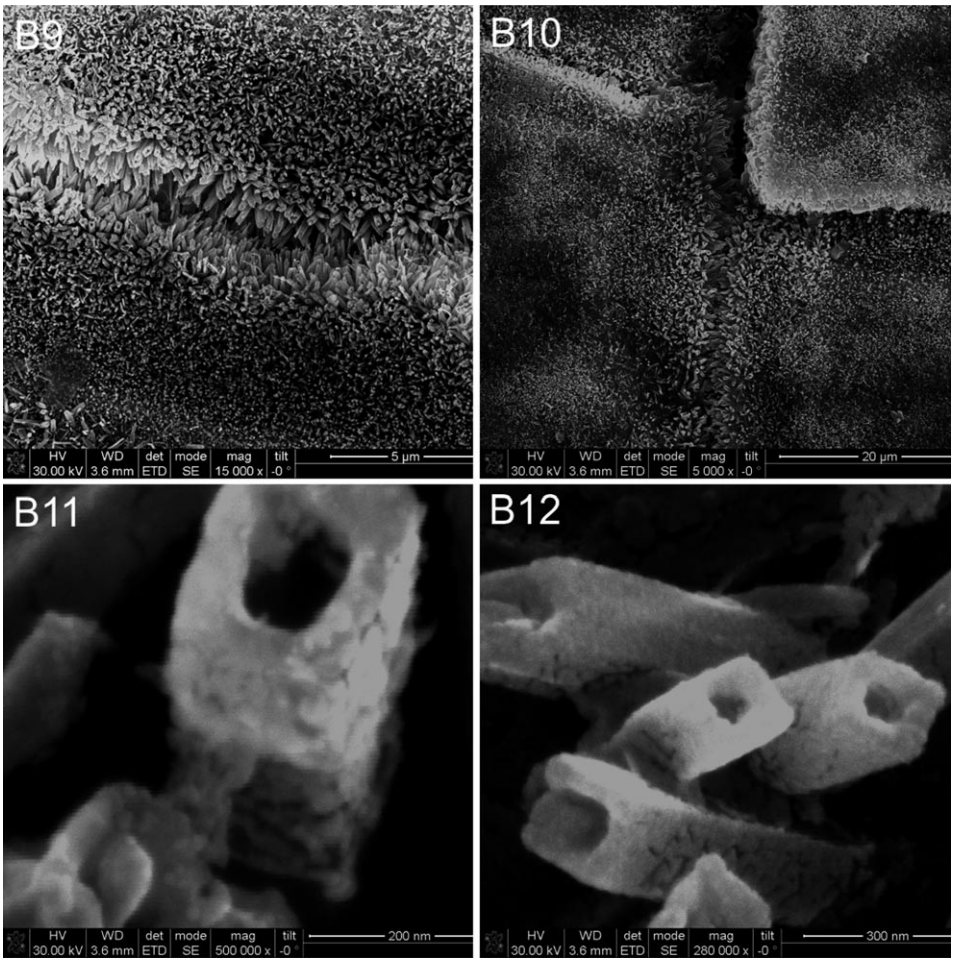

Fig. 2. *SEM Images of the surface of the deeply undercooled cryolite/alumina melt* (10 wt.-% of Al_2O_3) (*Nova 200 NanoLab-DualBeam™-SEM/FIB* system, *FEI Company*). Magnification: *B9* 15000 ×, *B10* 5000 ×, *B11* 500000 ×, and *B12* 250000 ×. The roughness of the outer walls of the nanotubes is caused by the presence of a thin Au layer.

nanotubes 'layer'. We utilized the *Nova-200-DualBeam*™ system (FEI) for the preparation of the individual lamella (*Fig. 5*).

The dependence of electron-penetration depth on the accelerating voltage and material density is well known. In our case, the density of the bulk material was calculated to be *ca.* 2 g/cm^3, and in combination with a 25 – 30 kV accelerating voltage, we could expect a penetration of electrons up to 8 – 10 µm under the sample surface. Along the penetration path, the electrons interact with matter which causes the production of X-rays. According to [12], for our conditions (density and accelerating voltage), we consider that the largest X-ray production occurs 400 – 600 nm under the

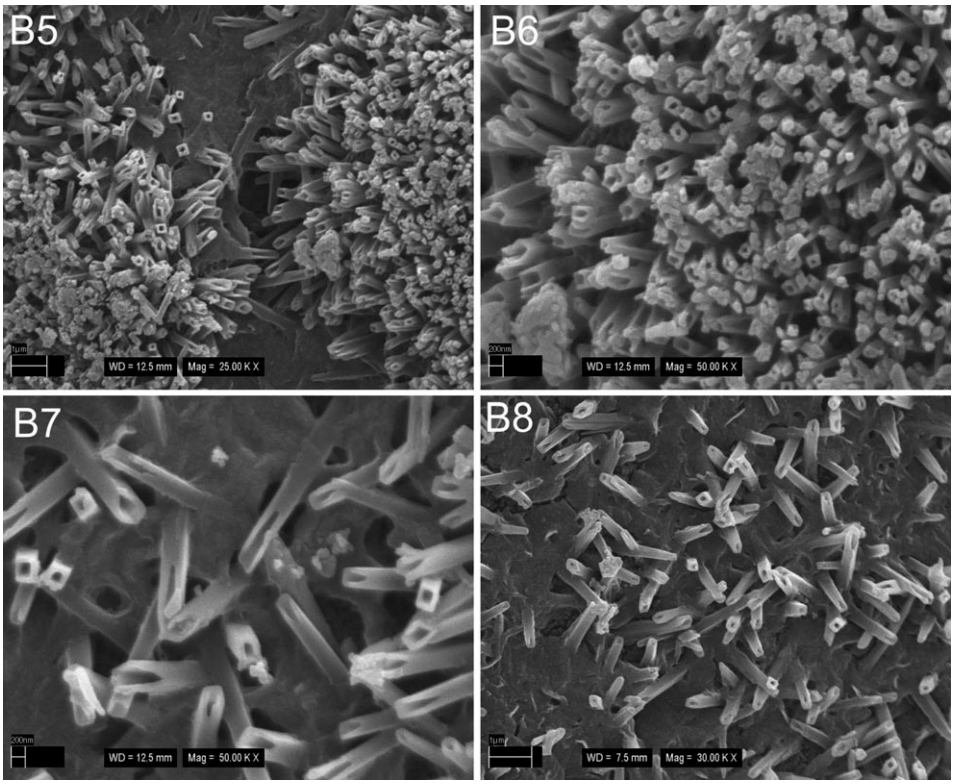

Fig. 3. *SEM Images of the surface of the deeply undercooled cryolite/alumina melt* (10 wt.-% of Al_2O_3), *after heating in the air at 600°* (*Zeiss* model *EVO 40 HV*, *Carl Zeiss SMT AG*, Germany). Magnification: *B5* 25000 ×, *B6* 50000 ×, *B7* 50000 ×, and *B8* 30000 ×.

sample surface, but the total X-ray generation volume is consistent with the penetration path of the electrons.

In the following, we will discuss the results obtained with both EDX approaches. In general, we have to take into account discontinuity of the nanotube layer due to the density distribution of the nanotubes at the surface of the bulk material and also the quite large volume of the nanotube cavities (*Fig. 2*, *B12*). As a consequence, it is difficult to target a large amount of nanotube matter for X-ray photons produced by the application of a perpendicular e-beam. In the case of the first approach where a perpendicular e-beam is used (*Fig. 4*), we obtained more information about the bulk material than about the nanotube matter (see *Table*).

The results obtained with the second method (*Fig. 5*) will now be discussed. In the process of lamella preparation, a thin layer of Pt was deposited on the top surface of the sample by electron-beam-induced deposition (EBID) for protection. In our case, the deposited Pt is an advantage for the protection of the nanotube layer and its filling with Pt. If we consider a more continuous space for X-ray generation and a tilted e-beam

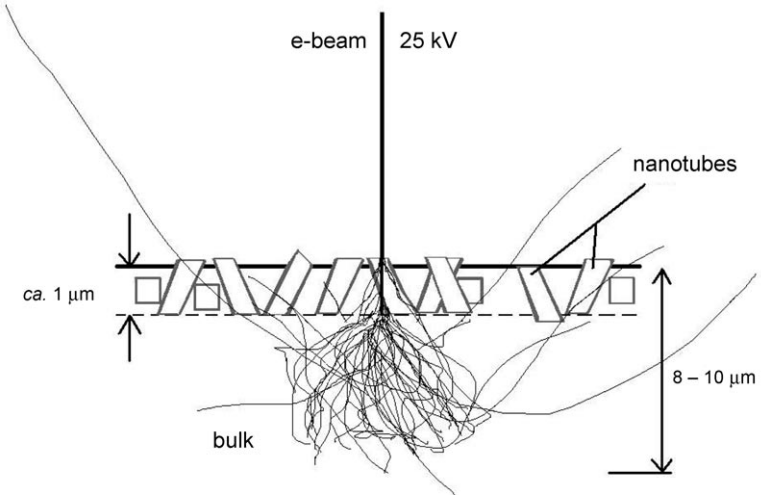

Fig. 4. *EDX Measurement recorded by the* EVO 40 HV *device* (*Carl Zeiss SMT AG*, Germany)

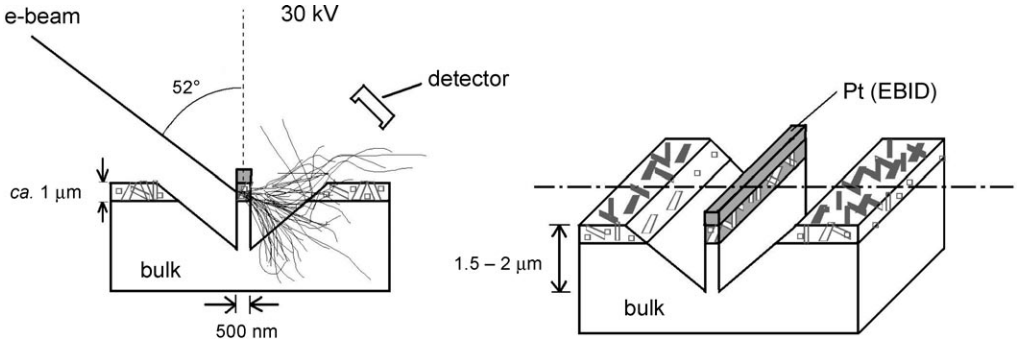

Fig. 5. *EDX Measurement recorded by the* Nova 200 DualBeam™ *system* (*FEI Company*). Pt(EBID) is a thin layer of Pt which was grown by electron-beam-induced deposition.

Table. *The Element Content of the 'Nanotubes' Reached by Using the Two EDX-Measurement Approaches,* i.e., *the* EDX-EVO-AO-HV (*Carl Zeiss SMT AG*) *and* EDX-Nova-200-DualBean™ (*FEI Company*) *System*

		Atom [%]				
		C	O	F	Na	Al
EDX-EVO 40 HV		9.23	26.8	43.7	10.8	9.4
EDX-Nova 200 DualBeam™	considering C-content	11.5	33.5	24.2	7.3	23.5
	not considering C-content		35.2	27.1	8.8	28.9

with good focusing on the side wall of the nanotube layer, then we can expect the largest production of X-ray right within the material of this layer.

Results of EDX for both methods are shown in the *Table*. One could expect (taking into account the information mentioned above) differences in the element contents between the bulk material and the nanotubes, as it was indeed observed in our EDX experiments. The Al-content in the 'nanotubes' against 'bulk' is evidently increased, and *vice versa*, the F-content is decreased. The C- and O-content in the 'nanotubes' and in the 'bulk' can be considered as being the same. However, we are still not able to exclude some influence of the bulk material on the EDX results (*Fig. 5*). Likewise, also some discrepancies (in the EDX analysis) could be present related to the relatively low atomic masses of the investigated elements. Because of that fact, we could not draw clear conclusions for the composition of the nanotubes. Actually, we are trying to get more precise informations by measuring the EDX spectra in a lifted-out lamella (perpendicular targeting of the e-beam on the nanotube layer on the side wall of a stand-free lamella) and by the investigation of the nanotube material by means of high-resolution (HR) transmission electron microscopy (TEM). The preparation of samples for HR-TEM is in progress.

X-Ray-Diffraction (XRD) *Analysis.* The study of solidified cryolite/alumina samples has a long scientific tradition because cryolite and alumina are the main constituents of the electrolyte for industrial aluminium electrolysis. The molten cryolite/alumina system represents a complex mixture of different ionic entities, ranging from simple Na cations to larger fluoroaluminate (AlF_6^{3-}, AlF_2^{5-}, AlF_4^-) and fluorooxoaluminate anions ($Al_2OF_6^{2-}$, $Al_2OF_8^{4-}$, $Al_2O_2F_2^{4-}$). However, the detailed structure of the complex anions in the melt is still controversial [13].

The results of XRD analysis of deeply undercooled cryolite/alumina melts (0, 10, 20, and 30 wt.-% of Al_2O_3) are given in *Fig. 6*. In the previous works [14–16] related to the XRD analysis of solidified cryolite/alumina samples (cooling rate hundreds K/s *vs.* 10^6 K/s in our case), only cryolite diffractions were found in the XRD patterns. The X-ray diffraction patterns of all our samples showed cryolite lines. The sample with 20 wt.-% of Al_2O_3 exhibited, along with cryolite, a very small diffraction signal from α-Al_2O_3. The sample with 30 wt.-% of alumina also showed relatively high intensity diffractions of α-Al_2O_3 ($=\alpha$-corundum). In both cases, there was an undissolved residuum of primary alumina in the sample. In the samples with 10 wt.-% of alumina and with 30 wt.-% of alumina, a very small unknown peak appeared which is probably related to the C impurities mentioned above.

IR Analysis. The IR spectra of deeply undercooled cryolite/alumina melts (0, 10, 20, and 30 wt.-% of Al_2O_3) have characteristic stretching vibrations typical for Al–F bonds (580–660 cm^{-1}) in cryolite [17] (*Fig. 7*). The spectra also exhibit absorptions of Al–O bonds in the AlO_4 tetrahedra (900–650 cm^{-1}) and AlO_6 octahedra (650–450 cm^{-1}) [18]. Aluminium oxide (corundum) has very strong vibrations mainly in the range 450–790 cm^{-1}; in our experiments, vibrations at 456, 502, 557, 600, 641, and 765 cm^{-1} were measured.

The vibrations in the present IR spectra (*Fig. 7*, *c* and *d*) at 765, 502, and *ca.* 460 cm^{-1} could be attributed to the undissolved primary alumina (detectable also by XRD). The spectra also contain vibrations at 806 and 706 cm^{-1}, which cannot be assigned either to cryolite or to undissolved alumina (corundum). A wide band with maxima at *ca.* 870 cm^{-1} is observed as well. This one is located in the AlO_4 tetrahedra. The vibration could come from an amorphous or micro(nano-)crystal-

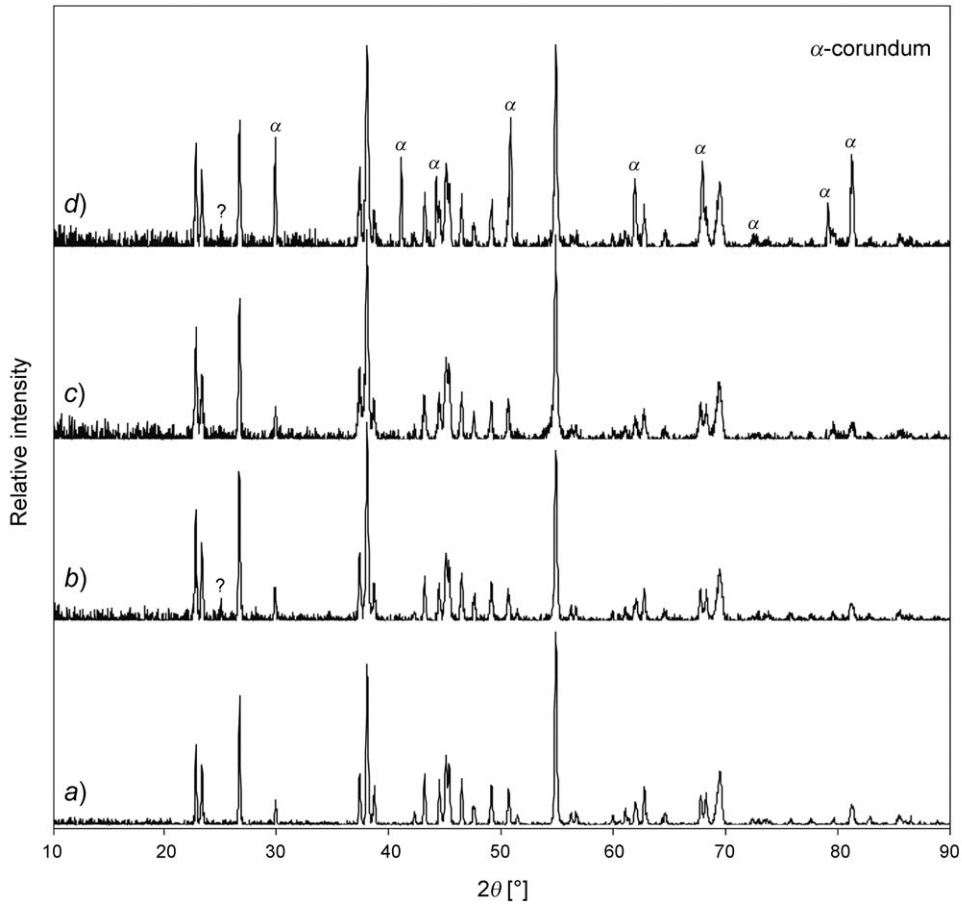

Fig. 6. *X-Ray powder diffraction patterns of the samples:* a) *quenched cryolite,* b) *quenched cryolite/alumina 90 : 10* (wt-%), c) *quenched cryolite/alumina 80 : 20* (wt.-%), d) *quenched cryolite/alumina 70 : 30* (wt.-%)

line phase (undetectable by XRD) formed by rapid quenching of cryolite/alumina melts.

Bache and *Ystenes* [19] also investigated solidified cryolite/alumina samples (cooling rate around hundreds K/s *vs.* 10^6 K/s in our case) by IR analysis. They reported that aluminium oxide does not exist as alumina in the quenched samples, but as oxofluorides. A similar result has been published also in [20].

Probably, there are no single fluorooxoaluminate species present in the deeply undercooled melts. We would rather expect formation of a mixture of several more or less complex entities, as suggested by the broad shoulder in the IR spectra of the samples prepared by RSP.

Only *Berg* and co-workers [21] observed *Raman* and IR spectra assigned to fluorooxoaluminate anion $Al_2OF_6^{2-}$ in the solid state at 25°. The spectra were obtained

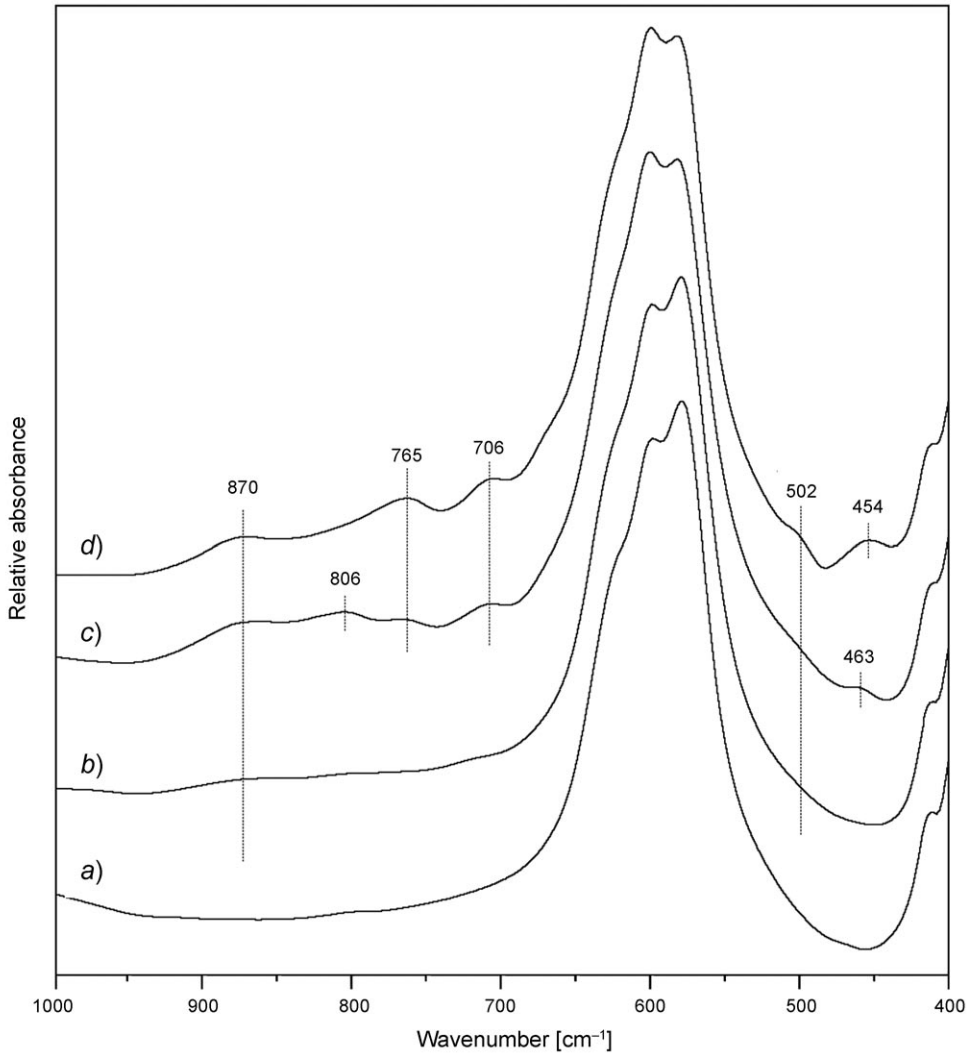

Fig. 7. *Infrared spectra of the samples:* a) *quenched cryolite,* b) *quenched cryolite/alumina 90 : 10* (wt.-%), c) *quenched cryolite/alumina 80 : 10* (wt.-%), d) *quenched cryolite/alumina 70 : 30* (wt.-%)

from premelted samples of 5 mol-% Na_2O and 5 mol-% AlF_3 in FLiNaK (NaF/KF/LiF). A wide band in the range 760–930 cm^{-1}, with a maximum at 809 cm^{-1}, and two clearly resolved shoulders at 785 and 890 cm^{-1} in the IR spectrum of this sample could be observed. These results [21] do not correspond with our IR analysis; however, a different system with a relatively low content of O-species was investigated. According to *Sterten* [22] (based on thermodynamic calculations), one could consider a majority of $Al_2OF_6^{2-}$ anions in systems with lower concentration of O-species (as in [21]), while, in systems with the highest concentration of O-species, dominance of $Al_2O_2F_2^{4-}$ anions could be expected (our case).

Conclusions. – From the observed properties, we can only speculate about the possible nature and structure of the RSP-prepared nanotubes. The nanotubes could consist of species such as fluoroaluminates (cryolite, Na_3AlF_4, or $NaAlF_4$), or a kind of alumina or a fluorooxoaluminate species ($Na_2Al_2OF_6$, $Na_4Al_2OF_8$, and $Na_2Al_2O_2F_4$). However, we could exclude the presence of fluoroaluminates in the nanotubes. In fact, we did not find any nanotubes of pure cryolite in the RSP-prepared samples.

There is also a possibility that nanotubes contain some kind of C-containing species like, for instance, aluminium carbide. Equally, alumina probably plays the role in the formation process of nanotubes on the surface of deeply undercooled melts (although the tubes do not consist of pure Al_2O_3 and likely contain Na- and C-atoms as well).

Amorphous nanotubes composed of Sr, Al, and O in an atomic ratio which corresponds to the stoichometric formula $SrAl_2O_4$ [23] could be found in the literature. These nanotubes preserve their tubular morphology as they change to the crystalline state upon high-temperature annealing (1300°, 4 h). The authors are also mentioning (TEM analysis) that nanotubes adopt a monoclinic structure that consists of a three-dimensional network of corner-sharing $\{AlO_4\}$ tetrahedra containing connected open channels. This result corresponds to the IR analysis of our nanotubes. However, the mentioned nanotubes are relatively different, having well-established cylindrical (prismal) features.

For further investigations of the morphology and structure of the nanotubes, transmission electron microscopy (TEM), high-resolution (HR) TEM, as well as energy-dispersive X-ray spectroscopy (EDX) of one nanotube will be employed. The separation of the individual nanotubes for these analyses will be done by a *NOVA-200-NanoLab-DualBeam*™ system. Also the separation of larger amounts of the nanotubes will be necessary for the investigation of the possibly interesting physical and chemical properties (optical, magnetic, electrical, reactivity, *etc.*).

Slovak Grant Agencies (APVV-51-008104, VEGA 2/7077/27, and *VEGA* 2/5096/27) are acknowledged for financial support.

Experimental Part

General. The following chemicals were used: hand-picked powdered cryolite from Greenland (m.p. 1009–1011°) and powdered Al_2O_3 (*Merck*, *p.a.*). Both chemicals were dried at 500° for several h before usage. Scanning electron microscopy (SEM): *Zeiss* microscope, model *EVO 40 HV* (*Carl Zeiss SMT AG*, Germany), equipped with a *Brooker-AXS* flesh detector *4010*. X-Ray diffraction (XRD): *Stoe-Stadi-P* diffractometer, equipped with a linear PSD (position-sensitive detector), and a curved Ge(111) primary beam monochromator. SEM and EDX analysis: *Nova-200-NanoLab-DualBeam*™*-SEM/FIB* system (*FEI Company*). IR Spectra: *Nicolet Magna-750* FT-IR spectrometer equipped with a *DTGS* detector; KBr pellets.

Preparation of Melts by RSP. The RSP apparatus consists of the inductive furnace and the rotating cooling Cu-wheel. The sample is placed in a graphite crucible glued into the quartz tube. At the bottom of the crucible is a small orifice for the outflow of the melt. The distance between the orifice and the rotating cylinder is *ca.* 0.2 mm. The quartz housing tube with the crucible and sample is filled with Ar. The apparatus permits the solidification of melts from the molten state (in our case around 100° above the melting point) to the solid by a cooling rate of *ca.* 10^6 K/s. Further general details of the technique are given in [4]. The rapidly solidified samples of different cryolite/alumina melts (0, 10, 20, and 30 wt.-% Al_2O_3) were prepared in this RSP apparatus. After the quenching, the sample prepared with 10 wt.-% of alumina was annealed (5 h), and then cooled spontaneously. Annealing of the sample was carried out by

heating at 600° for 5 h under open-air-atmosphere conditions. Just after thermal treatment of the sample, a few-nanometers-thick layer of Au was deposited on the sample surface by radio-frequency (rf) sputtering to avoid sample charging during electron-beam evaluation. The solidified samples were analyzed by SEM, EDX, XRD, and IR spectroscopy.

REFERENCES

[1] S. Iijima, *Nature (London, U.K.)* **1991**, *354*, 56.
[2] J. Duan, Q. Cao, S. Yang, H. Huang, X. Zhao, R. Zhang, G. Cheng, *J. Cryst. Growth* **2006**, *289*, 164.
[3] M. Suemitsu, T. Abe, H. Na, H. Yamane, *Jpn. J. Appl. Phys.* **2005**, *44*, 449.
[4] A. L. Jacobson, J. McKittrick, *Mater. Sci. Eng., R.* **1994**, *11*, 355.
[5] A. Ahlf, G. H. Frischat, *J. Am. Ceram. Soc.* **1989**, *72*, 1506.
[6] S. Shibat, *Mater. Res. Bull.* **1980**, *15*, 129.
[7] R. Tenne, L. Margulis, M. Genut, G. Hodes, *Nature (London, U.K.)* **1992**, *360*, 444; Y. Feldman, E. Wasserman, D. J. Srolovitz, R. Tenne, *Science (Washington, DC, U.S.)* **1995**, *267*, 222; N. G. Chopra, R. J. Luyken, K. Cherrey, V. H. Crespi, M. L. Cohen, S. G. Louie, A. Zettl, *Science (Washington, DC, U.S.)* **1995**, *269*, 966; P. M. Ajayan, O. Stephan, P. Redlich, C. Colliex, *Nature (London, U.K.)* **1995**, *375*, 564; Y. R. Hacohen, E. Grundbaum, R. Tenne, J. Sloan, J. L. Hutchison, *Nature (London, U.K.)* **1998**, *395*, 336; J. A. Hollingsworth, D. M. Poojary, A. Clearfield, W. E. Buhro, *J. Am. Chem. Soc.* **2000**, *122*, 3562; M. Nath, C. N. R. Rao, *J. Am. Chem. Soc.* **2001**, *123*, 4841; Y. Li, J. Wang, Z. Deng, Y. Wu, X. Sun, D. Yu, P. Yang, *J. Am. Chem. Soc.* **2001**, *123*, 9904; C. Ye, G. Meng, Z. Jiang, Y. Wang, G. Wang, L. Zhang, *J. Am. Chem. Soc.* **2002**, *124*, 15180; M. Brorson, T. W. Hansen, C. J. H. Jcobsen, *J. Am. Chem. Soc.* **2002**, *124*, 11582; M. Nath, C. N. R. Rao, *Angew. Chem.* **2002**, *114*, 3601; *Angew. Chem., Int. Ed.* **2002**, *41*, 3451; Y. R. Hacohen, R. Popowitz-Biro, E. Grundbaum, Y. Prior, R. Tenne, *Adv. Mater.* **2002**, *14*, 1075; J. Chen, Z. Tao, S. Li, *Angew. Chem.* **2003**, *115*, 2197; *Angew. Chem., Int. Ed.* **2003**, *42*, 2147; J. Chen, Z. Tao, S. Li, X. Fan, S. Chou, *Adv. Mater.* **2003**, *15*, 1379; S. Y. Hong, R. Popovitz-Biro, Y. Prior, R. Tenne, *J. Am. Chem. Soc.* **2003**, *125*, 10470; U. K. Gautam, S. R. C. Vivekchand, A. Govindaraj, G. U. Kulkarni, N. R. Selvi, C. N. R. Rao, *J. Am. Chem. Soc.* **2005**, *127*, 3658; C. Ye, Y. Bando, G. Shen, D. Goldberg, *Angew. Chem., Int. Ed.* **2006**, *45*, 4922 and refs. cited therein.
[8] Y. Liu, J. Dong, M. Liu, *Adv. Mater.* **2004**, *16*, 353.
[9] Y. Liu, M. Liu, *Adv. Funct. Mater.* **2005**, *15*, 57.
[10] W. Wang. Q. Li, M. Li, H. Lin, L. Hong, *J. Cryst. Growth* **2007**, *299*, 17.
[11] W. Merchan-Merchan, A. V. Saveliev, L. A. Kennedy, *Chem. Phys. Lett.* **2006**, *422*, 72.
[12] D. E. Newbury, D. C. Joy, P. Echlin, C. E. Fiori, J. I. Goldstein, 'Advanced Scanning Electron Microscopy and X-ray Microanalysis', Plenum, New York, 1986, p. 243.
[13] J. Thonstad, P. Fellner, G. M. Haarberg, J. Híveš, H. Kvande, A. Sterten, 'Aluminium Electrolysis, Fundamentals of the *Hall–Héroult* Process', 3rd edn., Aluminium-Verlag, Düsseldorf, Germany, 2001.
[14] P. A. Foster, *J. Electrochem. Soc.* **1959**, *106*, 971.
[15] E. Zintl, W. Morawietz, *Z. Anorg. Allg. Chem.* **1939**, *240*, 145.
[16] H. Ginsberg, A. Böhm, *Z. Elektrochem.* **1957**, *61*, 313.
[17] H. Moenke, 'Mineral-Spektren', Academie-Verlag, Berlin, 1962.
[18] P. Tarte, *Spectrochim. Acta A: Mol. Spectrosc.* **1967**, *23*, 2127.
[19] Ø. Bache, M. Ystenes, *Acta Chem. Scand.* **1989**, *43*, 97.
[20] M. Korenko, M. Kucharik, D. Janičkovič, *Chem. Pap.* **2008**, *62*, 219.
[21] M. H. Brooker, R. W. Berg, J. H. von Barne, N. J. Bjerrum, *Inorg. Chem.* **2000**, *39*, 4725.
[22] A. Sterten, *Electrochim. Acta* **1980**, *25*, 1673.
[23] C. Ye, Y. Bando, G. Shen, D. Goldberg, *Angew. Chem., Int. Ed.* **2006**, *45*, 4922.

Received March 28, 2008